Bioorganic & Medicinal Chemistry xxx (xxxx) xxx–xxx

Contents lists available at ScienceDirect

Bioorganic & Medicinal Chemistry

journal homepage: www.elsevier.com/locate/bmc

Anti-oligomerization sheet molecules: Design, synthesis and evaluation of inhibitory activities against α-synuclein aggregation

Hao Liu[a,1], Li Chen[a,1], Fei Zhou[a], Yun-Xiao Zhang[a,*], Ji Xu[b,*], Meng Xu[c], Su-Ping Bai[d,*]

[a] College of Chemistry and Molecular Engineering, Zhengzhou University, Daxue Road 75, 450052 Zhengzhou, China
[b] School of Basic Medical Science, Neuroscience Research Institute, Academy of Medical Sciences, Zhengzhou University, Kexue Road 100, 450001 Zhengzhou, China
[c] Department of Information of the First Affiliated Hospital, Zhengzhou University, Jianshe Road 1, 450052 Zhengzhou, China
[d] College of Pharmacy, Xinxiang Medical University, Jinsui Road 601, 453003 Xinxiang, China

ARTICLE INFO

Keywords:
α-Synuclein
Anti-aggregation
Inhibitor
Synthesis

ABSTRACT

Aggregation of α-synuclein (α-Syn) play a key role in the development of Parkinson Disease (PD). One of the effective approaches is to stabilize the native, monomeric protein with suitable molecule ligands. We have designed and synthesized a series of sheet-like conjugated compounds which possess different skeletons and various heteroatoms in the two blocks located at both ends of linker, which have good π-electron delocalization and high ability of hydrogen-bond formation. They have shown anti-aggregation activities in vitro towards α-Syn with IC50 down to 1.09 μM. The molecule is found binding in parallel to the NACore within NAC domain of α-Syn, interfering aggregation of NAC region within different α-Syn monomer, and further inhibiting or slowing down the formation of α-Syn oligomer nuclei at lag phase. The potential inhibitor obtained by our strategy is considered to be highly efficient to inhibit α-Syn aggregation.

1. Introduction

Parkinson's disease (PD) is one of the most common neurodegenerative diseases which affects approximately 1% of the population over 65 years of age, and the percentage has reached 1.7% in China.[1–4] The underlying molecular pathogenesis of PD involves multiple mechanisms: α-Synuclein (α-Syn) proteostasis, mitochondrial dysfunction, oxidative stress, calcium homeostasis, axonal transport and neuroinflammation. α-Syn monomer is a protein composed of 140 amino acids with high conformational flexibility. Although the precise function of α-Syn remains unclear, a growing number of studies have authenticated the effects of α-Syn on neuronal Ca^{2+} homeostasis, modulation of neurotransmitter release and regulation of dopamine synthesis, storage, clearance and efflux.[5] Futhermore, α-Syn has shown some other synaptic functions such as protein interactions, lipid transport, lipid packing and membrane biogenesis, and molecular chaperone activity.[6] In all PD cases, it was found that the intraneuronal protein aggregates in substantia nigra are largely consist of α-Syn. The aggregation process had been demonstrated when soluble α-Syn monomers form oligomers, then progressively aggregate to small protofibrils and eventually large, insoluble amyloid fibrils. The fibrils are neurotoxic and led to the death of dopaminergic neurons, which strongly support the notion that α-Syn is a key player in PD.[7–9] α-Syn consists of three main domains: an amphipathic *N*-terminal region (1–60), which has alpha-helical propensity and is involved in membrane binding; a hydrophobic central region (61–95), known as the non-amyloid-beta component (NAC), which is responsible for its aggregation; an acidic unstructured C-terminal region (96–140) enriched in negative charged and proline residues, which provides flexibility to the polypeptide (Fig. 1A).[10–12]

The NAC region is the most aggregation-prone region of α-Syn. The aggregation can be divided into three phases: the lag phase, the elongation phase, and the stationary phase. In the lag phase, α-Syn monomers accumulate to form oligomer nuclei, which is considered the rate-limiting step in the aggregation pathway. Once a certain number of nuclei have formed, they start to form fibrils *via* elongation phase, and stationary phase.[13] Many factors modulate the aggregation process of α-Syn, such as genetic factors, post-translational modifications, protein–protein interactions and environmental factors. The environmental factors include pH changes, metal ions, lipids, small molecules, etc.[14,15]

The solid-state NMR and micro-electron diffraction (Micro ED) measurements have revealed that the mature fibril contain several protofilaments with a cross β-sheets structure, in which individual β-strands run perpendicular to the fibril axis.[11,16–18] It has a proposed structure comprising a strongly protected region core with in-register β-

* Corresponding authors.
E-mail addresses: zhangyx@zzu.edu.cn (Y.-X. Zhang), xuji@zzu.edu.cn (J. Xu), baisuping@xxmu.edu.cn (S.-P. Bai).
[1] These authors contributed equally.

https://doi.org/10.1016/j.bmc.2019.05.032
Received 2 May 2019; Accepted 20 May 2019

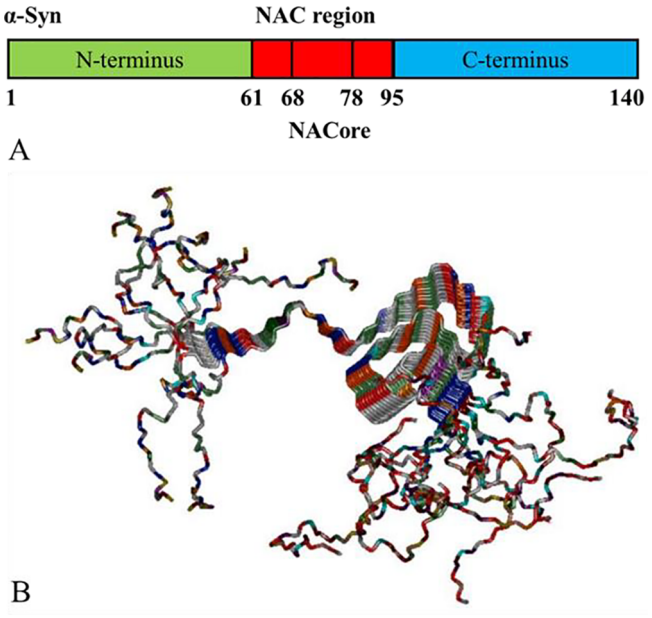

Fig.1. A) α-Syn domain structure: *N*-terminus (green), NAC region (61–95, red) including NACore (68–78) and C-terminus (blue). B) 3D structure of α-Syn fibril: residues 25 to 105 of 8 monomers showing the β-sheet alignment of each monomer in the fibril and the Greek-key topology of the core.

sheets in a Greek key motif (Fig. 1B).[19] The NACore (68–78) is the fibril forming core of the NAC domain of full-length α-Syn.

To date, an increasing number of peptide or antibody-based inhibitors have been shown to have inhibitory effects on α-Syn aggregation. In addition, many natural small molecules have been found to have good inhibitory effects including polyphenols such as exifone, rosmarinic acid, gallic acid, curcumin; flavonoids such as baicalein, delphinidin, (-)-epigallocatechin 3-gallate (EGCG), quercetin; congo red; vitamin A, etc.[20–27] The synthesized small molecular inhibitors have also been significantly reported such as phenothiazine analogs, LDS 798, 46a, etc.[28,29] In particular, Otzen *et al* developed a high-throughput screening assay combining SDS-stimulated α-Syn aggregation with FRET to reproducibly detect initial stages in α-Syn aggregation. Of the 58 compounds markedly inhibit α-Syn aggregation, the most effective ones were derivatives of (4-hydroxynaphthalen-1-yl) sulfonamide.[30] Similarly, Ventura *et al* identified a potent small molecule (SynuClean-D) *via* high-throughput screening. SynuClean-D significantly reduces the in vitro aggregation of wild type α-Syn. This compound prevents fibril propagation in protein-misfolding cyclic amplification assays and decreases the number of α-Syn inclusions in human neuroglioma cells (Scheme 1).[31]

By comparing the structural characteristics of these molecules, it is found that most compounds possess a conjugate and sheet structure with strong π-electrons delocalization and hydrogen bonding property. Based on these present evidences, our goal is to design suitable small molecules, which have strong binding force with the NACore and interfering the formation of β-sheets structure, blocking the formation of oligomer nuclei in the lag phase, and further preventing the development of α-Syn fibrillation. In this paper, we report the design, synthesis of a series of sheet-like conjugated compounds with different skeleton and various heteroatom, and their inhibitory activities against α-Syn aggregation.

2. Results and discussion

2.1. Chemistry

The serie 1 compounds were designed as benzoxazole or benzimidazole conjugated pyridine linked by diene (**3a-3q**, Scheme 2). Starting from commercial available 2-chloroacetonitrile, ethyl-2-chloroacetimidate hydrochloride (**Int 1**) was prepared. (*E*)-3-(pyridin-4-yl) acrylaldehyde (**Int 2)** and (*E*)-3-(pyridin-2-yl)acrylaldehyde **(Int 3)** were prapared through Aldol condensation of pyridylaldehyde with acetaldehyde. The key intermadiates 2-(chloromethyl)benzoxazoles and 2-(chloromethyl)benzimidazoles, **1a-1i** were obtained *via* substituted *o*-phenylenediamine or *o*-aminophenol condensed with **Int 1** in high yields. Phosphonium chlorides **2a-2i** were synthesized by reacting **1a-1i** with triphenylphosphine. Compounds **3a-3q** were synthesized from **2a to -2i** and **Int 2** or **Int 3** *via* Wittig reaction in medium yields.[32–34] NMR data analysis shown these target molecules possess full-trans structure.

The series 2 compounds were designed as pyridine conjugated benzamide derivatives and substituted benzene linked by dienone (**5a-5o**, Scheme 3). Starting from commercial available 4-acetylbenzoic acid and substituted amines, the key intermadiates, amides **4a-4g** and **4h-4j** were prepared under DCC and DMAP in high yield.[35–37] Compounds **5a-5g** and **5h-5j** were synthesized from **4a to 4g** or **4h-4j** and **Int 2** *via* Aldol reaction under CH_3OH-CH_3ONa in medium yields. Similarly, compounds **5k-5o** were obtained from *p*-substituted acetophenone and **Int 2** *via* Aldol reaction under EtOH-NaOH in medium yields. NMR data analysis confirm that the dienone linker in **5a-5o** possess full-trans structure.

The serie 3 compounds were designed as pyridine conjugated substituted benzene and benzoic acid derivatives linked by 1,4-divinylbenzene (**8a-8n**, Scheme 4). Starting from commercial available 4-methylpyridine and terephthalaldehyde, (*E*)-4-(2-(pyridin-4-yl)vinyl) benzaldehyde (**Int 4)** was prepared *via* Aldol condensation, and when 4-methylpyridine was excess, the bilaterally addition product **8** formed as main product. The intermadiates *p*-substitued benzyl bromide **6a-6d** and **6e-6j** were prepared through different methods. The former was prepared by direct bromination on *p*-substitued toluene with NBS, and the latter was prepared by esterification of 4-bromomethylbenzoic acid with alcohols under DCC-DMAP. Phosphonium bromides **7a-7j** were synthesized by reacting **6a-6j** with triphenylphosphine. Compounds **8a-8j** were synthesized from **7a to 7j** and **Int 4** *via* Wittig reaction in medium to high yields.[38,39] Compounds **8l-8o** were prepared from *p*-substituted aniline and pyridinylvinylstyrylbenzoic acid **8k** *via* amidation. Compound **8k** was from hydrolysis of **8e**. These target molecules have trans structure confirmed by NMR.

2.2. Biological evaluation

To investigate the inhibitory activities of the three series compounds against α-Syn aggregation, thioflavin T (ThT) fluorescence assays were utilized to detect the kinetic of aggregation. ThT, a fluorescent dye, is weakly fluorescent in the presence of monomeric α-Syn in the lag phase of α-Syn monomers accumulating to form oligomer nuclei or in an α-Syn fibril-free system. Inversely, in the presence of α-Syn fibrils, ThT is able to bind to the groove of β-sheet protein chain parallel to the fibril axis and fix the rotation around C−C bond in ThT molecule, thereby resulting the increase of ThT fluorescence.[26,28,29] Understandably, ThT fluorescence intensity can quantitatively reflect the kinetics and abilities of compounds inhibiting towards the aggregation of α-Syn.

Initially, ThT fluorescence detection parameters were optimized according to previous report.[29] The ThT fluorescence maximum emission wavelength was obtained at 482 nm (λ_{em} = 482 nm) under excitation light wavelength at 450 nm (λ_{ex} = 450 nm) by scanning the emission wavelength of free ThT, ThT-monomeric α-Syn and ThT-fibrils respectively, and it should be noted that no increase in fluorescent emission was observed in free ThT system as well as ThT-monomeric α-Syn.

Next, the concentration of compound as inhibitor was optimized, which was incubated with 40 μM α-Syn solution in 0.1 M PBS for 3 days, and then added 20 μM ThT to the system. Choosing the previously synthesized compounds (series 1) as models, **3a**, **3c** and **3d**

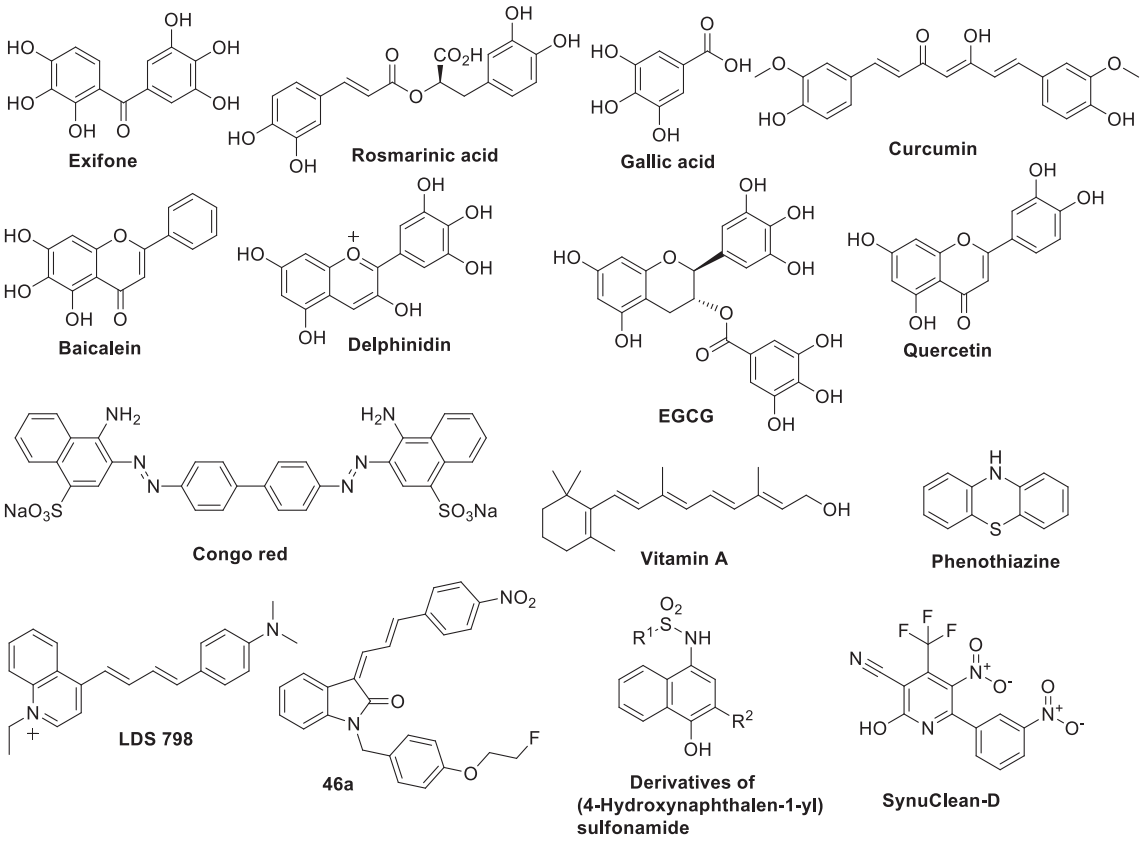

Scheme 1. Reported natural and synthesized small molecular inhibitors on α-Syn aggregation.

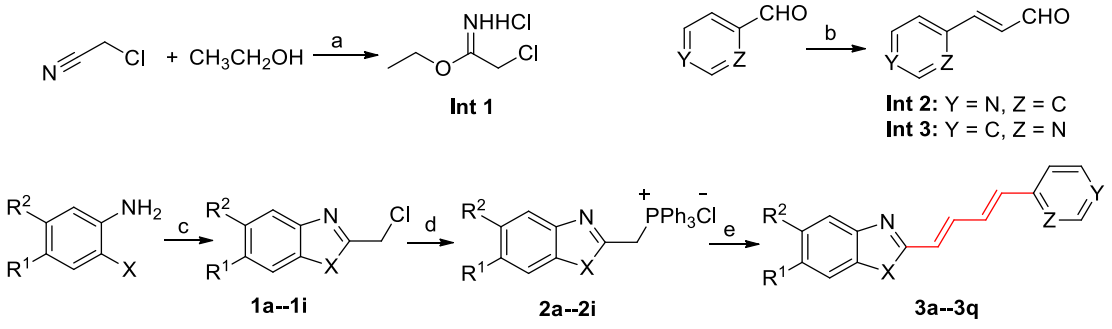

3a: X = O, Y = N, Z = C, R^1 = H, R^2 = H
3b: X = O, Y = N, Z = C, R^1 = H, R^2 = CH_3
3c: X = O, Y = N, Z = C, R^1 = H, R^2 = Br
3d: X = O, Y = N, Z = C, R^1 = F, R^2 = H
3e: X = O, Y = N, Z = C, R^1 = Cl, R^2 = H
3f: X = NH, Y = N, Z = C, R^1 = H, R^2 = NO_2
3g: X = NH, Y = N, Z = C, R^1 = H, R^2 = H
3h: X = NCH_3, Y = N, Z = C, R^1 = H, R^2 = H
3i: X = NTS, Y = N, Z = C, R^1 = H, R^2 = H

3j: X = O, Y = C, Z = N, R^1 =H, R^2 =H
3k: X = O, Y = C, Z = N, R^1 = H, R^2 = CH_3
3l: X = O, Y = C, Z = N, R^1 = H, R^2 = Br
3m: X = O, Y = C, Z = N, R^1 = F, R^2 = H
3n: X = O, Y = C, Z = N, R^1 = Cl, R^2 = H
3o: X = NH, Y = C, Z = N, R^1 = H, R^2 = NO_2
3p: X = NH, Y = C, Z = N, R^1 = H, R^2 = H
3q: X = NCH_3, Y = C, Z = N, R^1 = H, R^2 = H

Scheme 2. Synthesis of **3a-3q**. Reagents and conditions: a) absolute EtOH, HCl (g), Et_2O, 0 °C, 5.5 h, 81%; b) DCM, TBAB, K_2CO_3, CH_3CHO (40%), 0 °C, 5 h, 46%; c) DCM or CH_3OH, **Int 1**, r. t., 6 h, 75–80%; d) triphenylphosphine, toluene, 120 °C, 12 h, 60–67%; e) DMF, **Int 2** or **Int 3**, CH_3ONa, r. t., 5 h, 52–57%.

were set respectively to three concentration gradients, 1 μM, 30 μM and 100 μM. The fluorescence intensity was obtained by subtracting the PBS background. The blank group was fluorescence intensity of the tested system without inhibitor (compound), and thereby obtained the maximal fluorescence intensity. The value of blank group fluorescence intensity was set as 1 (100%). The ratio of the measured fluorescence intensity of the tested system within compound to that of blank group was difined as the relative fluorescence intensity. In fact, there was a positive correlation between the percent reduction of relative fluorescence intensity and the inhibitory activity of the evaluated compound. The results shown that the value of relative fluorescence intensity was dose-dependent with concentration of compounds, but at the higher concentration (100 μM), the fluorescence intensity did not shown significant decrease (Fig. 2A). As a result, 30 μM was chosen as an

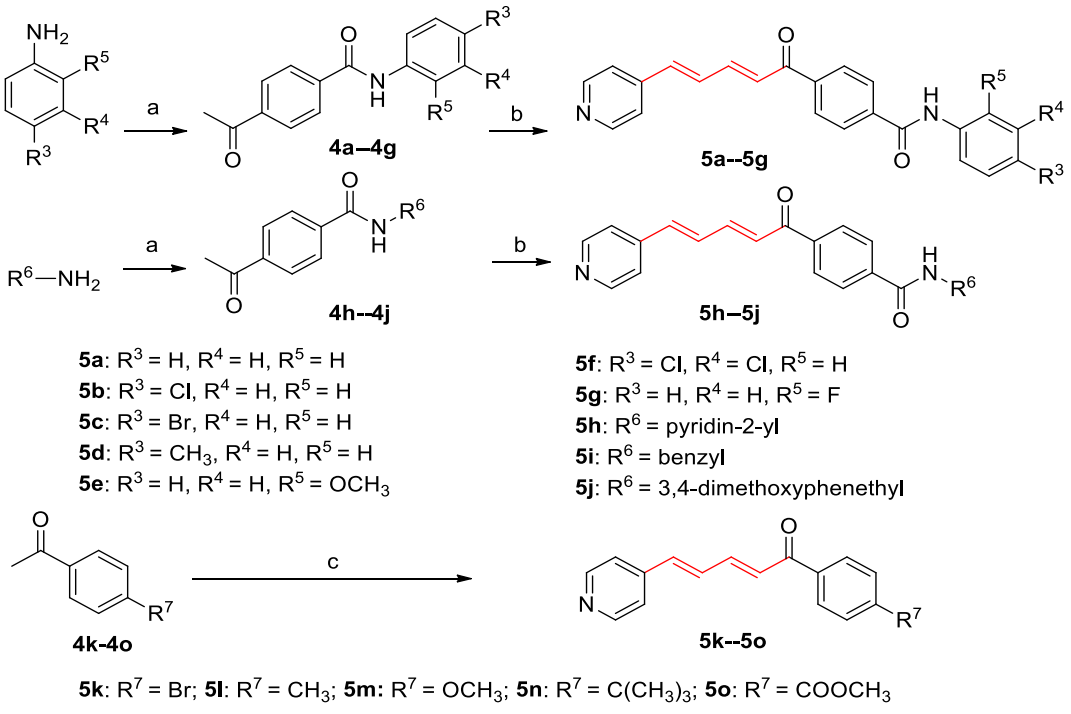

Scheme 3. Synthesis of **5a-5o**. Reagents and conditions: a) DCM, 4-acetylbenzoic acid, DCC, DMAP, 0 °C, 12 h, 80–94%; b) CH_3OH, CH_3ONa, **Int 2**, 0 °C, 12 h, 50–64%; c) EtOH, NaOH, **Int 2**, 0 °C-r. t., 4 h, 40–60%.

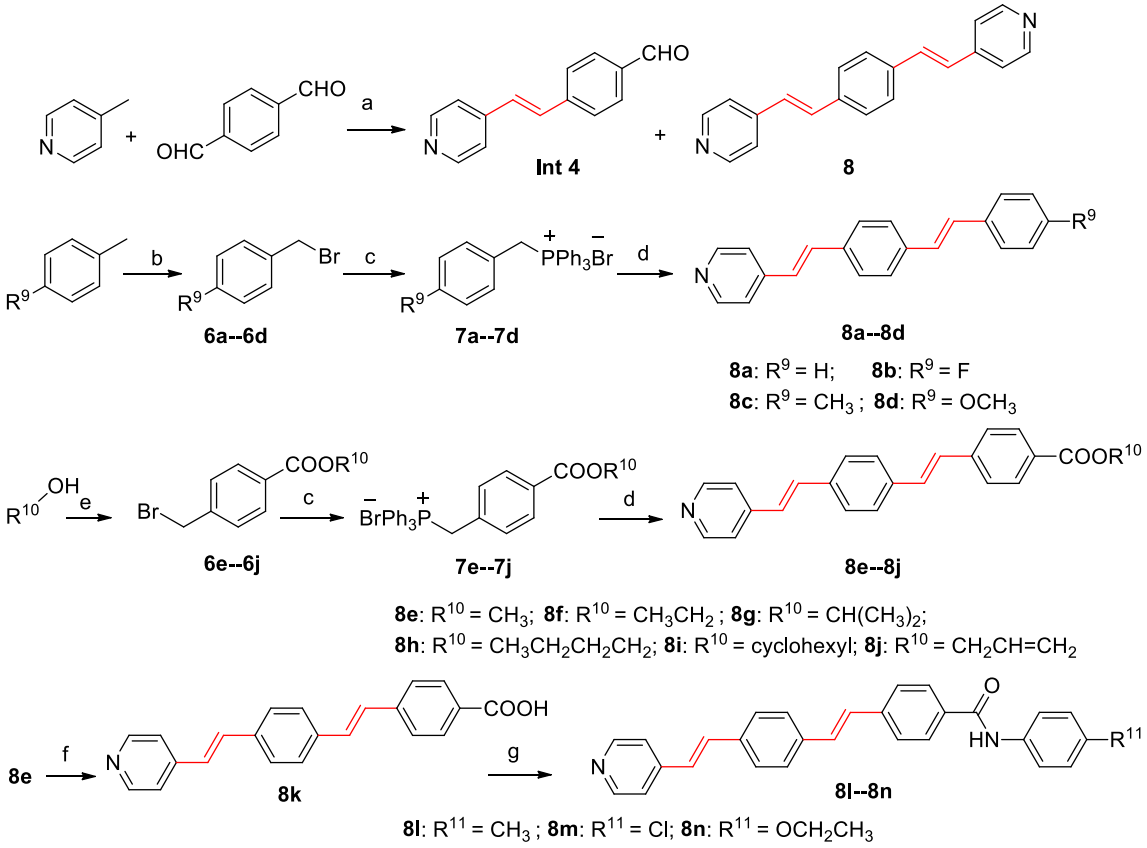

Scheme 4. Synthesis of **8-8n**. Reagents and conditions: a) AC_2O, reflux, 6 h, 4-methylpyridine:terephthalaldehyde = 1:1(mol/mol), 85% of **Int 4**; 4-methylpyridine:terephthalaldehyde = 2.5:1, 88% of **8**; b) CCl_4, NBS, reflux, 3 h, 60–70%; c) triphenylphosphine, toluene, 120 °C, 12 h, 70–80%; d) DCM, **Int 4**, NaOH, H_2O, r. t., 4 h, 60–70%; e) DCM, 4-bromomethylbenzoic acid, DCC, DMAP, 0 °C, 12 h, 70–80%; f) NaOH, H_2O, 60 °C, 6 h, 85%; g) DCM, *p*-substituted aniline, DCC, DMAP, 0 °C, 12 h, 70–84%.

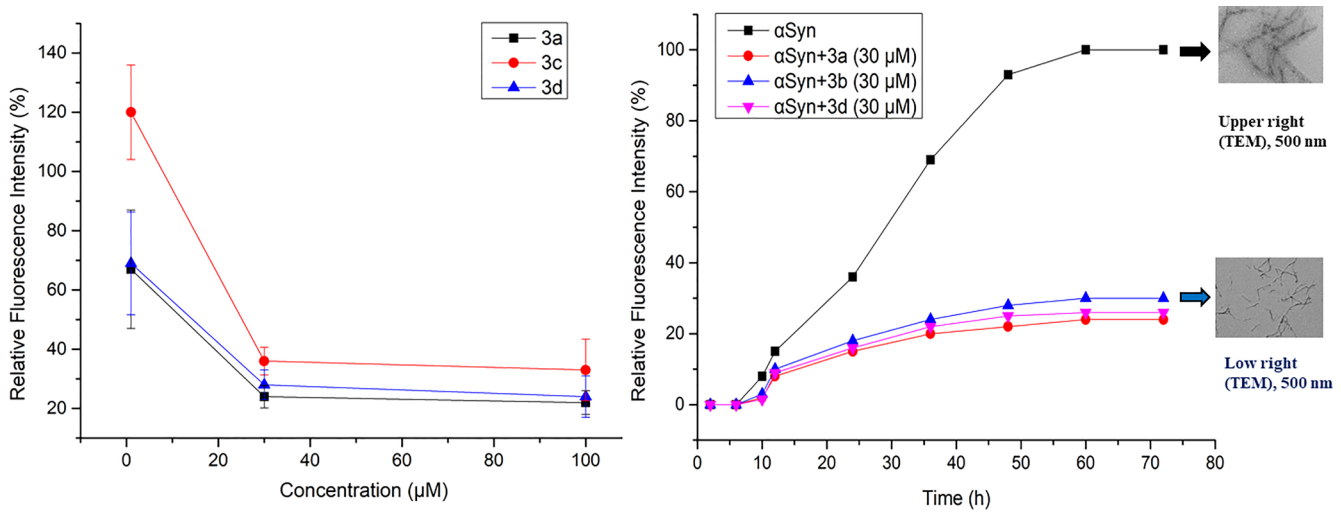

Fig. 2. A) Compound concentration optimization. **3a**, **3c** and **3d** were respectively incubated with 40 μM α-Syn solution in 0.1 M PBS (pH = 7.4) for 72 h at three concentration gradients, 1 μM, 30 μM and 100 μM. Their relative fluorescence intensities were obtained after adding 20 μM ThT to the system. B) Fibrillation kinetics of 40 μM α-Syn in the absence or presence of **3a**, **3b** and **3d** at 30 μM monitored by relative fluorescence intensity in vitro. Each value is mean of three replicates. The images on the right were TEM morphologies of α-Syn aggregation (500 nm). 40 μM α-Syn was incubated alone for 72 h (upper right), 40 μM α-Syn was incubated in the presence of 30 μM **3b** for 72 h (lower right).

appropriate concentration to apply in the following evaluations. Furthermore, the inhibitory kinetic of these compounds to α-Syn fibrillation was investigated under the optimized conditions above. The relative fluorescence intensity was measured in 40 μM α-Syn solution incubated with 30 μM of **3a**, **3b** and **3d** respectively (Fig. 2B). The formation kinetics of fibrils without inhibitor (black curve) displayed three phases: (i) lag phase, the formation of β-sheets nucleus during the first 7 h, (ii) elongation phase, the logarithmic increase of β-sheets during 7–48 h, and (iii) stationary phase, the saturation of β-sheets during 48–72 h. The addition of compounds caused slower increase of the relative fluorescence intensity over the time, which indicated the inhibitory effect of these compounds on α-Syn fibril formation. To confirm the relative fluorescence intensity results, the morphology of α-Syn during the conformation transition with and without inhibitor were observed by transmission electron microscope (TEM) (Fig. 2B right). The upper right TEM image in Fig. 2B shown the image of α-Syn alone after 72 h incubation, which exhibit the typically bundled fibrils formed. The lower right TEM image in Fig. 2B shown the image of α-Syn after 72 h incubation with compound **3b** at 30 μM. Compared to the bundled fibrils above, the fibrils appeared thinner, revealing an effective inhibition of α-Syn fibrillation by **3b**.

Under the same condition described above, most compounds of series 1, series 2 and series 3 were evaluated for their relative fluorescence intensities. The results (Fig. 3) demonstrated that the relative fluorescence intensities of these compounds are less than 100%, from 24.0% to 62.3%. Understandably, the lower relative fluorescence intensity is corresponding to the higher inhibitory activity against α-Syn aggregation. In order to describe the inhibition activity more conveniently, the relative fluorescence intensity was transformed to α-Syn aggregation inhibition ratio by the formula: α-Syn aggregation inhibition ratio = 100% (blank group)-x% (compound group). The ratio value intuitively reflected the inhibitory activity of compound (Table 1).

From Table 1, the series 1 conmpouds have shown the inhibitory ratio towards α-Syn aggregation from 37.7% to 76.0%. Compounds **3a**, **3b**, **3d**, **3j** and **3o** displayed more than 70% inhibition ratio. Series 1 compounds are comprised of benzoxazole or benzimidazole and pyridine moieties, which were conjugated by trans diene. Firstly, **3a** and **3j** displayed similar inhibition ratio (76.0% vs 75.5%), suggesting pyridin-2-yl and pyridin-4-yl had similar effect. For the benzoxazole block, substituent at position 5, such as methyl and bromo groups slightly reduce inhibitory activities. This trend was identified by comparing the inhibition ratio of **3a**, **3b** and **3c** (76.0%, 70.0% and 63.7%), as well as **3j**, **3k** and **3l** (75.5%, 58.7% and 56.5%). Similarly, the substituent groups at position 6, such as fluoro and chloro also reduced the inhibitory activities from the downtrend in **3a**, **3d** and **3e** (76.0%, 71.7% and 69.7%), as well as in **3j**, **3n** and **3m** (75.5%, 39.7% and 37%). Secondly, for the benzimidazole block, the inhibitory activities are slightly reduced than benzoxazole block by comparing the inhibition ratio of **3a** and **3g** (76.0% and 62.7%), as well as of **3j** and **3p** (75.5% and 59.0%). And more, substituent at position 1 on the benzimidazole block, such as methyl and tosyl, have little influence on their inhibitory activities by comparing the inhibition ratio of **3g**, **3h** and **3i** (62.7%, 56.5% and 62.7%). Interestingly, the compoud **3o**, 5-nitro-1*H*-benzimidazole conjugated 2-pyridine has displayed an increased inhibitory activity (73.7%).

Series 2 compounds are comprised of two building blocks of pyridine and substituted benzene linked with full trans dienone and some analogues showed medium to high inhibition activities (58.5% to 75.5%). Compound **5b** has displayed higher activity (75.5%) and **5f**, **5e**, **5g** and **5j** shown the moderate activities as 60.0%, 65.0%, 65.0% and 69.0% respectively. The SAR study revealed that benzamide block is favorable to increase inhibition ratio, especially *p*-chlorobenzamide (**5b**).

Series 3 compounds are consisted of two building blocks conjugated by trans 1,4-divinylbenzene. One block is pyridine and the other block is substituted benzene or benzoic acid derivative. Compound **8** has two same blocks of pyridine. These compounds also displayed inhibitory activities from 42.5% to 76.0%. Compound **8j** possessing the allyl benzoate block gave the highest ratio of 76%. On the other hand, **8k**, **8e**, and **8n**, which possess benzoic acid, methyl benzoate and benzamide, showed lower ratio of 54.0%, 48.2% and 56.2%. In addition, **8d** (substituted benzene block) and **8** also showed moderate to low activities from 53.0% to 42.5%.

Next, some representative analogues with higher inhibitory activities were chosen to perform IC_{50} study (Table 2). The results indicated that the linkers did not demonstrate distinct differences for the inhibitory activities. This is in agreement with our hypothesis, that the function groups on both sides play key roles for high activity. In addition, the calculated LogP values of **3a**, **3b**, **3e** and **3o** suggest their

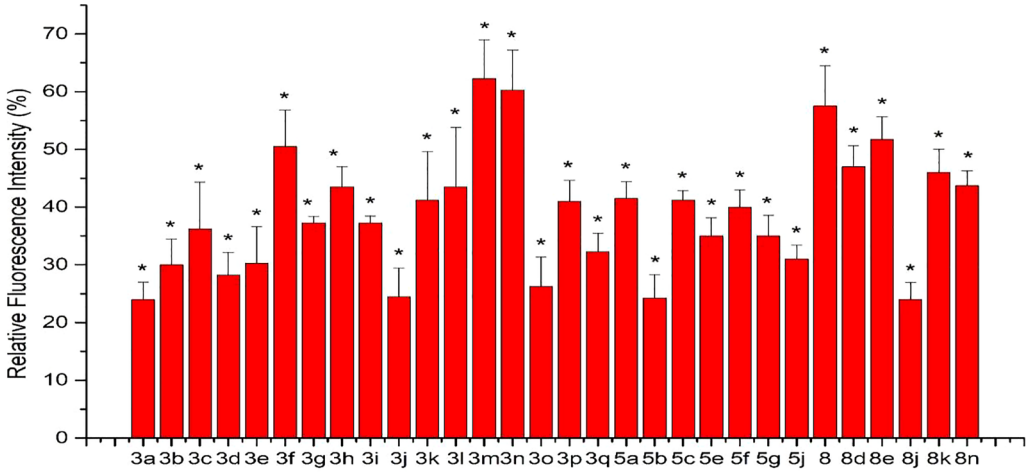

Fig. 3. The relative fluorescence intensities of compounds **3a-8n.** Each compound (30 μM) was incubated with 40 μM α-Syn solution in 0.1 M PBS (pH = 7.4) for 3 days and then 20 μM ThT was added. Each value is mean of three replicates. (∗) p less than 0.05.

Table 1
The structure activity relationship study of series 1–3 compounds on α-Syn aggregation.

Cmpd.	Structure	Log P[a]	Ratio[b] (%)	Cmpd.	Structure	Log P	Ratio (%)
Series 1 compounds	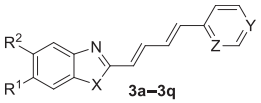 **3a–3q**						
3a	X = O, Y = N, Z = C, R^1 = H, R^2 = H	2.90	76.0	**3j**	X = O, Y = C, Z = N, R^1 = H, R^2 = H	3.33	75.5
3b	X = O, Y = N, Z = C, R^1 = H, R^2 = CH_3	3.39	70.0	**3k**	X = O, Y = C, Z = N, R^1 = H, R^2 = CH_3	3.81	58.7
3c	X = O, Y = N, Z = C, R^1 = H, R^2 = Br	3.73	63.7	**3l**	X = O, Y = C, Z = N, R^1 = H, R^2 = Br	4.16	56.5
3d	X = O, Y = N, Z = C, R^1 = F, R^2 = H	3.06	71.7	**3m**	X = O, Y = C, Z = N, R^1 = F, R^2 = H	3.48	37.7
3e	X = O, Y = N, Z = C, R^1 = Cl, R^2 = H	3.46	69.7	**3n**	X = O, Y = C, Z = N, R^1 = Cl, R^2 = H	3.88	39.7
3f	X = NH, Y = N, Z = C, R^1 = H, R^2 = NO_2	3.67	49.5	**3o**	X = NH, Y = C, Z = N, R^1 = H, R^2 = NO_2	3.90	73.7
3g	X = NH, Y = N, Z = C, R^1 = H, R^2 = H	2.83	62.7	**3p**	X = NH, Y = C, Z = N, R^1 = H, R^2 = H	3.25	59.0
3h	X = NCH_3, Y = N, Z = C, R^1 = H, R^2 = H	3.07	56.5	**3q**	X = NCH_3, Y = C, Z = N, R^1 = H, R^2 = H	3.49	67.7
3i	X = NTs, Y = N, Z = C, R^1 = H, R^2 = H	4.76	62.7				
Series 2 compounds	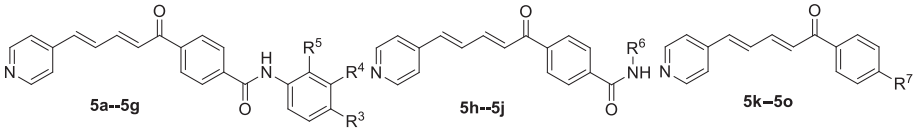 **5a--5g** **5h--5j** **5k–5o**						
5a	R^3 = H, R^4 = H, R^5 = H	4.63	58.5	**5i**	R^6 = benzyl	3.64	n.d.
5b	R^3 = Cl, R^4 = H, R^5 = H	5.18	75.7	**5j**	R^6 = 3,4-dimethoxyphenethyl	3.66	69.0
5c	R^3 = Br, R^4 = H, R^5 = H	5.45	58.7	**5k**	R^7 = Br	3.59	n.d.
5d	R^3 = CH_3, R^4 = H, R^5 = H	4.06	n.d[c].	**5l**	R^7 = CH_3	3.25	n.d.
5e	R^3 = H, R^4 = H, R^5 = OCH_3	4.50	65.0	**5m**	R^7 = OCH_3	2.64	n.d.
5f	R^3 = Cl, R^4 = Cl, R^5 = H	5.74	60.0	**5n**	R^7 = $C(CH3)_3$	4.47	n.d.
5g	R^3 = H, R^4 = H, R^5 = F	5.11	65.0	**5o**	R^7 = $COOCH_3$	2.58	n.d.
5h	R^6 = 2-pridinyl	2.95	n.d.				
Series 3 compounds	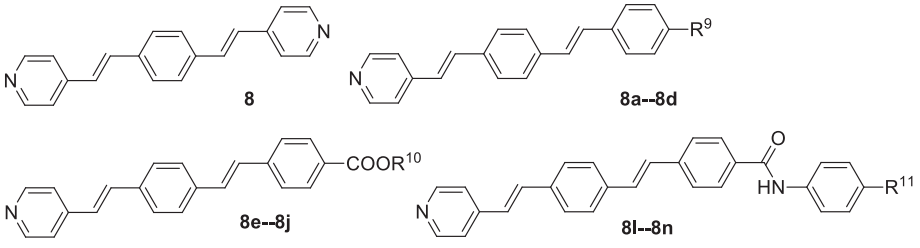 **8** **8a--8d** **8e--8j** **8l--8n**						
8	–	3.74	42.5	**8h**	R^{10} = $CH_2CH_2CH_2CH_3$	6.14	n.d.
8a	R^9 = H	5.08	n.d.	**8i**	R^{10} = cyclohexyl	6.45	n.d.
8b	R^9 = F	5.24	n.d.	**8j**	R^{10} = CH_2CH = CH_2	5.59	76.0
8c	R^9 = CH_3	5.57	n.d.	**8k**	R^{10} = H	4.64	54.0
8d	R^9 = OCH_3	4.95	53.0	**8l**	R^{11} = CH_3	6.37	n.d.
8e	R^{10} = CH_3	4.90	48.2	**8m**	R^{11} = Cl	6.44	n.d.
8f	R^{10} = CH_2CH_3	5.24	n.d.	**8n**	R^{11} = OCH_2CH_3	6.10	56.2
8g	R^{10} = $CH(CH_3)_2$	5.55	n.d.				

[a] Calculated by ChemBioDraw 12.0; [b] the α-Syn aggregation inhibition ratio of compound at 30 μM; [c] not determined

Table 2
IC_{50} and calculated binding energy and inhibition constant (K_i) to polypeptide 4RIL of the representative analogues.

Cmpd.	Structure	IC_{50} (μM)	Binding energy[a] (kcal/mol)	K_i[b] (mM)
3a	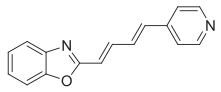	1.85 ± 0.12	−3.33	3.6
3b	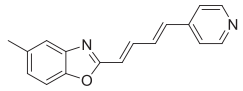	4.43 ± 0.22	−3.46	2.92
3e	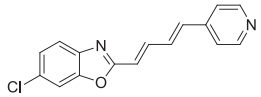	2.19 ± 0.03	−3.49	2.75
3o	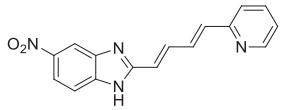	1.09 ± 0.14	−4.04	1.09
5b	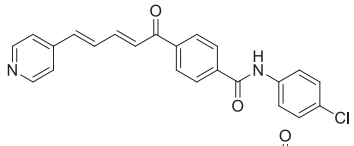	2.05 ± 0.29	−4.02	1.13
8j	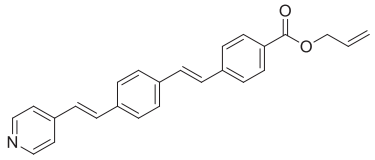	3.13 ± 0.12	−3.96	1.25

[a] bonding energy between compound and polypeptide 4RIL calculated by AutoDock 4.2; [b] inhibition constant calculated by AutoDock 4.2.

lipophilicities are within the desired range (from 1 to 5), so that they are acceptable with a high possibility of crossing the blood-brain-barrier.

2.3. Computational chemistry studies

Further modeling studies were carried out by AutoDock 4.2. According to the report of Rodriguez and coworkers,[18] the nanocrystal stacking structure of NACore in α-Syn, a polypeptide of GAVVTGVTAVA (4RIL), was measured by Micro ED. It was found that it is very similar to the core skeleton of α-Syn fibril, which is the molecular basis for the aggregation and fibrosis of α-Syn. In spite of the binding form of inhibitor with NACore is unclear, we performed the modeling studies to find its possible and stable binding form. To understand the interaction between the potential inhibitor molecule and β-sheet in α-Syn, the calculation was performed as following. The 3D structure of 4RIL was obtained from PDB databases. Taken 4RIL polypeptide as rigid and molecule as flexible, combined Lamarck genetic algorithm with semi-empirical free energy evaluation method, the optimum binding mode of molecule to 4RIL polypeptide was obtained by semi-flexible docking *via* changing the orientation of molecule and 4RIL and the direction of flexible bond between them. The binding energy and inhibition constant were listed in Table 2. Generally, for a ligand molecule docking with a receptor, the higher absolute value of bonding energy, the higher inhibitory activity of the ligand, which is agreement to the lower IC_{50} value. On the other hand, the larger inhibition constant K_i result to more unstable binding or weaker inhibitory activity. Table 2 shown that compound **3o** had the largest absolute value of bonding energy (−4.04 kcal/mol) and smaller K_i value (1.09 mM), corresponding to the smallest IC_{50} value (1.09 μM).

In detail, the docking results showed that molecule **3o** and polypeptide chain 4RIL was parallel in spatial orientation, and the hydrogen bond was formed between carbonyl O of V74 and N—H of imidazole in **3o**, at the same time, the hydrophobic Pi-alkyl interaction was formed between methyl group of A76 and benzene rings, and two Pi-sigma

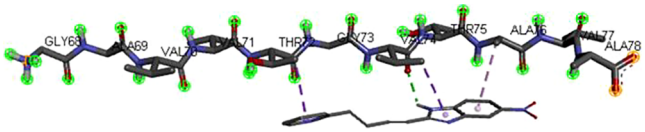

Fig. 4. Spatial relative positions and optimal interaction of **3o** and 4RIL polypeptide chain.

were formed including between methyl group of T72 and the pyridine ring, as well as between methyl group of T74 and imidazole ring, which enhanced the binding ability and improved the stability for **3o** and 4RIL (Fig. 4).

Base on the results above, we try to propose a hypothetical mechanism of sheet-like conjugated molecule inhibiting α-Syn oligomerization and fibrillation. According to previous report,[13] the α-Syn aggregation process was going through three phases. The rate-limiting step was at lag phase, the formation of small nuclei (oligomer). Rather, inhibiting or slowing down the nuclei formation should be the critical approach. The proposed mechanism was displayed in Fig. 5. In the NAC domain of full-length α-Syn, the NACore was the fibril-forming core, on which the sheet-like conjugated molecule such as **3o**, tended to bind parallelly. This binding was considered to be reversible and it will interfere the formation of nuclei, slowing down the oligomerization process, further inhibiting fibrillation of α-Syn protein.

3. Conclusions

We have designed and synthesized 47 compounds possessed of sheet-like conjugated structural moiety. The two blocks located at both ends of linker, contained various substituted aryl ring and aromatic heterocyclic ring, which provided robust π-electron delocalized effect and strong hydrogen bonding properties. These analogues have shown anti-aggregation activities *in vitro* towards α-Syn with IC_{50} down to 1.09 μM. We have proposed an anti-aggregation mechanism. The molecules inhibit or slow down the formation of α-Syn oligomer nuclei by

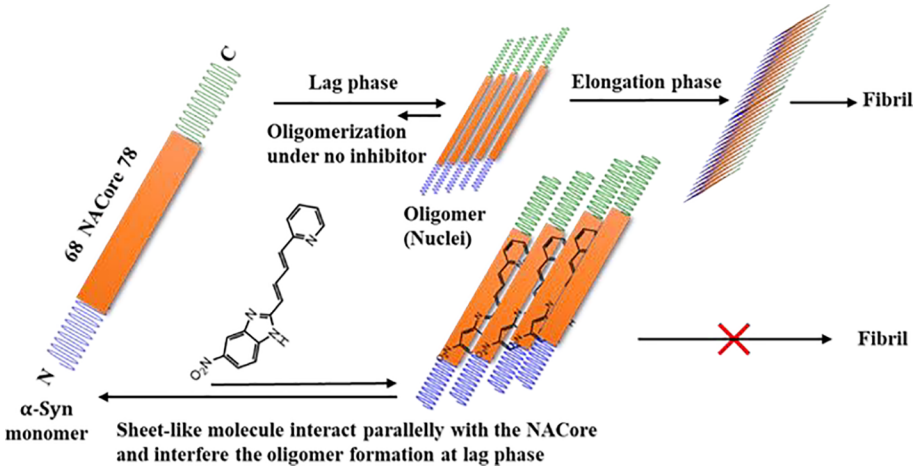

Fig. 5. Proposed anti-aggregation mechanism. Sheet-like molecular inhibitor interact parallelly with the NACore, especially at T72-A76, and interfere the formation of oligomer nuclei at lag phase.

reversible binding to the NACore within NAC domain of full-length α-Syn. This study will be beneficial to PD therapies targeting the toxic α-Syn oligomers in the near future.

Acknowledgments

This work supported by the National Natural Science Foundation of China (31500833 and 81870956), Science and Technology Planning Project of Henan Province of China (192102310141) and the Project for Disciplinary Group of Psychology and Neuroscience in Xinxiang Medical University.

Appendix A. Supplementary data

Supplementary data to this article can be found online at https://doi.org/10.1016/j.bmc.2019.05.032.

References

1. Shvadchak VV, Afitska K, Yushchenko DA. *Angew Chem Int Ed.* 2018;57:5690–5694.
2. Ma CL, Su L, Xie JJ, Long JX, Wu P, Gu L. *J Neural Transm.* 2014;121:123–134.
3. Kalia LV, Lang AE. *Lancet.* 2015;386:896–912.
4. Dorsey ER, Elbaz A, Nichols E, et al. *Lancet Neuro.* 2018;17:939–953.
5. Butler B, Sambo D, Khoshbouei H. *J Chem Neuroanat.* 2017;83–84:41–49.
6. Burre JJ. *Parkinsons Dis.* 2015;5:699–713.
7. Kim C, Lee SJ. *J Neurochem.* 2008;107:303–316.
8. Melki RJ. *Parkinson's Dis.* 2015;5:217–227.
9. Poewe W, Seppi K, Tanner CM, et al. *Nat Rev Dis Primers.* 2017;3:17013.
10. Broersen K, van den Brink D, Fraser G, Goedert M, Davletov B. *Biochem.* 2006;45:15610–15616.
11. Atsmon-Raz Y, Miller Y. *J Phys Chem B.* 2015;119:10005–10015.
12. Villar-Piqué A, Lopes da Fonseca T, Outeiro TF. *J Neurochem.* 2016;139(Suppl 1):240–255.
13. Arosio P, Knowles TP, Linse S. *PCCP.* 2015;17:7606–7618.
14. Deleersnijder A, Gerard M, Debyser Z, Baekelandt V. *Trends Mol Med.* 2013;19:368–377.
15. Ghosh D, Mehra S, Sahay S, Singh PK, Maji SK. *Int J Biol Macromol.* 2017;100:37–54.
16. Vilar M, Chou HT, Luhrs T, Maji SK, Riek-Loher D, Verel R, Manning G, Stahlberg H, Riek R. *Proc Natl Acad Sci USA.* 2008;105:8637–8642.
17. Van der Wel PCA. *Solid State Nucl Magn Reson.* 2017;88:1–14.
18. Rodriguez JA, Ivanova MI, Sawaya MR, et al. *Nature.* 2015;525:486–490.
19. Tuttle MD, Comellas G, Nieuwkoop AJ, et al. *Nat Struct Mol Biol.* 2016;23:409–415.
20. Masuda M, Suzuki N, Taniguchi S, et al. *Biochem.* 2006;45:6085–6094.
21. Mochizuki H, Choong CJ, Masliah E. *Neurochem Int.* 2018;119:84–96.
22. Liu Y, Carver JA, Calabrese AN, Pukala TL. *BBA.* 1844;2014:1481–1485.
23. Zhu M, Han S, Fink AL. *BBA.* 1830;2013:2872–2881.
24. Hu Q, Uversky VN, Huang M, et al. *BBA.* 1862;2016:1883–1890.
25. Cheng B, Gong H, Xiao H, Petersen RB, Zheng L, Huang K. *BBA.* 1830;2013:4860–4871.
26. Zhao J, Liang Q, Sun Q, et al. *RSC Adv.* 2017;7:32508–32517.
27. Quideau S, Deffieux D, Douat-Casassus C, Pouysegu L. *Angew Chem Int Ed Engl.* 2011;50:586–621.
28. Chu W, Zhou D, Gaba V, et al. *J Med Chem.* 2015;58:6002–6017.
29. Yu L, Cui J, Padakanti PK, et al. *Bioorg Med Chem.* 2012;20:4625–4634.
30. Kurnik M, Sahin C, Andersen CB, et al. *Cell Chem Biol.* 2018;25:1389–1402.
31. Pujols J, Pena-Diaz S, Lazaro DF, et al. *Proc Natl Acad Sci U S A.* 2018;115:10481–10486.
32. Rodríguez JM, Dolors Pujol M. *Tetrahedron Lett.* 2011;52:2629–2632.
33. Ananthakrishnan SJ, Kumar BS, Somanathan N, Mandal AB. *RSC Adv.* 2013;3:8331–8340.
34. Ribeiro Morais G, Vicente Miranda H, Santos IC, Santos I, Outeiro TF, Paulo A. *Bioorg Med Chem.* 2011;19:7698–7710.
35. Young DD, Connelly CM, Grohmann G, Deiters A. *J Am Chem Soc.* 2010;132:7976–7981.
36. Bashary R, Khatik GL. *Bioorg Chem.* 2018;82:156–162.
37. Zhang YX, Zhang AQ, Tian JS, Loh TP. *Org Biomol Chem.* 2013;11:8387–8394.
38. Abbate S, Bazzini C, Caronna T, et al. *Tetrahedron.* 2006;62:139–148.
39. Soriano-Moro G, Percino MJ, Sanchez AL, Chapela VM, Ceron M, Castro ME. *Molecules.* 2015;20:5793–5811.